technologies

Article

PHB/PEG Nanofiber Mat Obtained by Electrospinning and Their Performances

Nguyen Hong Thanh [1,*], Roman Olekhnovich [1], Vera Sitnikova [1], Arina Kremleva [2], Petr Snetkov [1] and Mayya Uspenskaya [1,*]

[1] Institute BioEngineering, ITMO University, Kronverkskiy Prospekt, 49A, Saint Petersburg 197101, Russia
[2] Institute of Advanced Data Transfer System, ITMO University, Saint Petersburg 197101, Russia
* Correspondence: hongthanhtropical@gmail.com (N.H.T.); mv_uspenskaya@mail.ru (M.U.)

Abstract: In this work, a nanofiber mat based on PHB/PEG with various PEG contents was obtained by electrospinning process. The thermal and mechanical properties of the PHB/PEG nanofiber mat were investigated. In addition, PHB/PEG nanofiber mats were characterized by Fourier transforms infrared spectroscopy (FTIR), differential scanning calorimetry, thermogravimetric analysis, X-ray diffraction, and water contact angle measurement. It was shown that, by increasing the PEG contents from 1 to 4%, the average diameter of PHB nanofibers decreased from 1177 nm to 1101 nm, corresponding to 2% PEG, then the diameter of the fiber increased again from 1101 nm to 1136 nm, corresponding to 4% PEG. Tensile strength increased from 3.6 MPa to 4.4 MPa, then decreased from 4.4 MPa to 2.9 MPa. Thermogravimetric analysis showed a difference in the process of thermal degradation of nanofiber mats. The degree of crystallinity measured by XRD and DSC methods gives different values at some points. The results demonstrated that adding PEG improved the mechanical properties, hydrophobicity, porosity, and thermal stability of the PHB fiber mat, which showed that the PHB/PEG nanofiber mat has great potential for air filtration or water filtration.

Keywords: polyhydroxybutyrate; polyethylenglycol; nanofibers mat; electrospinning

Citation: Thanh, N.H.; Olekhnovich, R.; Sitnikova, V.; Kremleva, A.; Snetkov, P.; Uspenskaya, M. PHB/PEG Nanofiber Mat Obtained by Electrospinning and Their Performances. *Technologies* **2023**, *11*, 48. https://doi.org/10.3390/technologies11020048

Academic Editor: Yury A. Skorik

Received: 4 March 2023
Revised: 20 March 2023
Accepted: 21 March 2023
Published: 24 March 2023

1. Introduction

Nanofibers are one-dimensional nanomaterials of fiber shape with a diameter of tens to hundreds of nanometers [1]. Therefore, nanofibers present a high surface area-to-volume ratio, interconnected nanoporosity, high porosity, small pore size, and low density [2]. Some techniques include drawing techniques, spinneret-based tunable engineered parameter (STEP) method, phase separation, self-assembly, template synthesis, freeze-drying synthesis, and interfacial polymerization of nanofibers [3]. Currently, electrospinning is the most widely used method for the preparation of nanofibers [4]. The advantages of electrospun nanofibers include small structure size; large specific surface area; and control over morphology, porosity, and composition using simple equipment. Because of those advantages, the electrospun nanofiber is widely applied in many fields, such as air filtration [5], antibacterial [6], oil/water separation [7], tissue engineering scaffolding [8], drug delivery [9], reinforced polymer composites [10], and sensors [11]. Electrospinning technology especially shows breakthroughs in some specific fields, such as medicine. Mengna et al. [12] were grafted with a nitric oxide (NO) donor (nitrosoglutathione, GSNO) to provide one type of NO loading cargo. The mats were found to have a prolonged NO release profile for 408 h with a maximum release of 1.0 μmol/L, which had a significant effect on killing bacteria and destructing biofilms. Ye et al. [13] manufactured nanofiber-constructed yarns (NYs) from polycaprolactone (PCL) and silk fibroin (SF) with blocks of different amount ratios by combining conventional electrospinning technique with hand winding and stretching post-treatment and also demonstrated their great potential for the tissue engineering and regenerative medicine applications.

Besides the above advantages, electrospun nanofiber still has some disadvantages that can be mentioned, such as poor mechanical properties, which result from interfibrillar slips, porous structures, and the isotropic conformation of functional groups in fibers [14]. Having poor mechanical properties restrict their application in large-scale industrial applications, especially in liquid filtration. Low mechanical stiffness of the nanofiber mats can lead to filter split [15]. The low mechanical properties of the nanofiber mat can be explained by the nanofiber mat's high porosity and the isotropically arranged nanofibers. Furthermore, the bond between the independent nanofibers is not stable. Many methods have been used to improve nanofiber mats' mechanical properties, such as mixing with other polymers, heating [16], and chemical cross-linking [17].

Polyhydroxybutyrate (PHB) is one of the popular polymers of the PHA family. PHB has received significant attention due to its potential environmental, pharmaceutical, and biomedical applications because of its biodegradability, thermoplasticity, biocompatibility, and non-toxicity. In addition, PHB showed great potential to replace petroleum-based polymers. Some researchers have already thought of PHB-based nanofiber mats for filter media. Mas et al. [18] successfully prepared microfiltration porous nanofibers mat from polyhydroxybutyrate and poly(hydroxybutyrate-co-hydroxyvalerate) with 9% and 22% valerate contents for pervaporation ethanol from the water. The results showed that with an increase in the flux from 0.008 to 0.027 Kg m^{-2} h^{-1}, the separation factor increased from 5.0 to 12.6 in favor of water permeation. Marova et al. [19] fabricated a PHA-based nanofibers mat to remove microorganisms from water. The results showed that PHA-based nanofibers mat could adhere up to 90% Bacillus subtilis to fibers. However, the disadvantages of PHB-based nanofibers mat include the fact that it lacks mechanical strength compared with conventional plastic, low permeability, and low porosity limiting the applicability of PHB-based nanofibers mat in water purification.

Many methods have been applied to improve the disadvantages of PHB-based nanofibers mat, such as copolymerization and blending with natural polymers (cellulose, gelatin) or synthetic polymers (PE, PP, PVC). In many works, Polyethylene glycol (PEG) is used to provide more permeability and mechanical properties of PHB-based nanofibers mat. Parra et al. [20] investigated blends of poly (3-hydroxybutyrate) (PHB) with poly (ethylene glycol) (PEG), (PHB/PEG), in different proportions of 100/0, 98/2, 95/5, 90/10, 80/20, and 60/40 wt%. The results demonstrated that an increase in the PEG content reduced the tensile strength from 28 $\pm$ 3 MPa to 13 $\pm$ 4 MPa and increased the elongation at break of pure PHB from 9% to 31%. Tomietto et al. [21] made PHBHV/PEG-based nanofibers mat by evaporation-induced phase separation (EIPS) for bacteria filtration from water. They highlighted that the nanofibers mat with PEG8000 shows the best performances so far, with pure water permeabilities over 200 L m^{-2} h^{-1} bar^{-1} associated with the bacteria rejection of 99.95%, which makes it promising for MF applications. Rodman et al. [22] fabricated and researched the characterization of the PHB/PEG-based film. The results showed that the crystallinity reduces from 70.1% for PHB films to 41.5% for its composite with a 30% (*w*/*w*) loading of PEG2000. Blending also enabled manipulation of the material properties, increasing film flexibility with an extension to break of 2.5 for PHB films and 8.3 for films containing 30% (*w*/*w*) PEG106. Significant changes in the film surface properties, as measured by porosity, contact angles, and water uptake, were also determined as a consequence of the blending process, and these supported greater adhesion and proliferation of neural-associated olfactory ensheathing cells (OECs).

In this study, PHB was mixed with PEG by electrospinning to improve the mechanical properties and hydrophilic properties of PHB and optimized for filtration application.

2. Materials and Methods

2.1. Materials

PHB (mark Aonilex X151A) granule was supplied by Kaneka Corporation (Westerlo-Oevel, Belgium) (Mw 500,000–600,000). The selection of PHB with the above molecular weight is because of the industry's availability, so if nanofiber mats are made from this PHB,

the possibility of nanofiber mats application in practice will be higher. PEG (Mw 8000) by Zavod sitanolov (Russia), chloroform «EKOS-1» (Russia) was used because the PHBV nanofiber mats with PEG8000 show the best performances so far, with pure water permeabilities over 200 $L \cdot m^{-2} \cdot h^{-1} \cdot bar^{-1}$ associated to the rejection of 99.95%, where bacteria makes it promising for MF applications [21].

2.2. Sample Preparation (Fabrication of PHB/PEG Nanofiber Mat)

First, we selected the optimal PHB concentration by changing the PHB solution concentration from 4% to 12%.

A polymer solution of PHB/PEG was prepared by dissolving the polymer granule in the chloroform ($CHCl_3$). PHB concentration is fixed at 8% of the total mass solution. PEG concentration varies from 1% to 4% of the total mass solution. The selection of PEG content varied from 1% to 4%, according to Tomietto et al. [19], which showed that 2% PEG and 5% PHB/PEG content showed high bacterial removal efficiency of the nanofiber mat. The solution was stirred for one hour at 40 °C until PHB/PEG dissolved completely. Viscosity was determined by Anton Paar Physica MCR-502 rheometer (Austria) with cylindrical measuring system CC27/T200/SS. The results are shown in Figure 1.

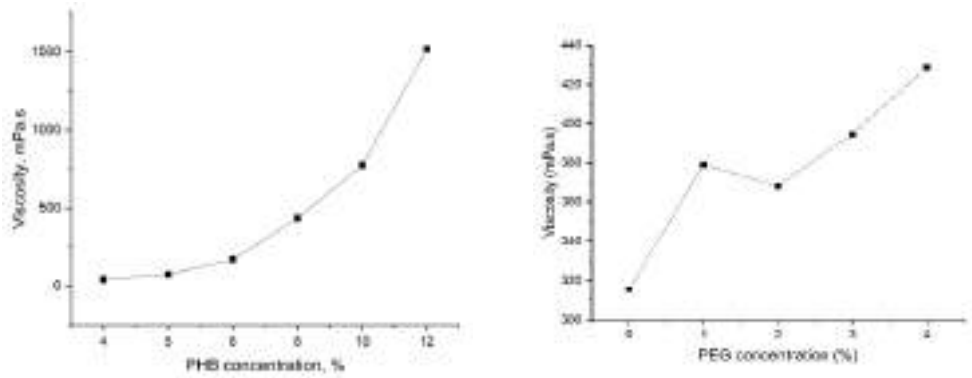

(**a**) (**b**)

Figure 1. The viscosity of PHB solution (**a**) and PHB/PEG solution (**b**).

PHB/PEG nanofiber mats were obtained by using a nanofiber electrospinning system NANON-01A (MECC Co., Ltd., Fukuoka, Japan) using rotating drum collectors (diameter 200 mm, length 200 mm) at the room temperature of 25 °C, the humidity of 60%, and the rotational speed of the drum of 500 rpm. The PHB/PEG solution was filled into a 10 ml syringe; the applied voltage was 30 kV; the flow rate of the solution was 0.5 mL/h; the distance from the tip of the needle to the drum collector was 15 cm. After successful electrospinning, PHB/PEG nanofiber mats were stored for one day under laboratory conditions to allow the complete evaporation of the solvent.

2.3. Characterization of PHB/PEG Nanofibers Mat

2.3.1. Morphology of Electrospun PHB Fibers

A measuring microscope Olympus STM6 was used for a detailed study of the structure of the fiber. ImageJ [23,24] program was used to analyze photographs and determine the mean fiber diameter.

2.3.2. Fourier Transform Infrared Spectroscopy (FTIR)

FTIR spectra of PHB/PEG nanofiber mat were recorded using a Tensor 37 spectrometer (Bruker, Germany) using a MIRacle Pike Technologies ATR attachment equipped with a diamond-coated ZnSe crystal. The measurements were performed with a spectral resolution of 2 cm^{-1} in the 4000−600 cm^{-1} and averaged over 32 scans.

2.3.3. Thermal Properties

The thermal properties were performed using a TG 209 F1 Libra (Netzsch, Germany) in the temperature range of 25 °C to 900 °C with an increasing rate of 10 °C/min in a nitrogen atmosphere with a flow rate of 40 mL/min.

The DSC measurements (DSC 204 F1 Phoenix, NETZSCH) were performed from 25 to 175 °C at a heating rate of 10 °C/min and then cooled to −30 °C at a cooling rate of 3 °C/min and reheated to 200 °C at a heating rate of 10 °C/min for the second heating run. The glass transition temperatures (Tg) of samples were taken from the midpoint of the stepwise specific heat increment. The degree of crystallinity (X_{DSC}) for samples was determined according to the following Equation (1) [25]:

$$X_{DSC} = \frac{\Delta H_m - \Delta H_c}{\omega \Delta H_m^0} \times 100\% \quad (1)$$

where ΔH_m and ΔH_c are the enthalpies of melting and cold crystallization, respectively, ω and ΔH_m^0 are the weight fraction of PHB (or PEG) and melting enthalpy of 100% crystalline PHB (or PEG). ΔH_m^0 enthalpy of melting for 100% crystalline PEG (202.4 J/g) [26,27] and PHB (146 J/g) [28,29].

2.3.4. XRD Analysis

XRD analysis was performed using an X-ray diffractometer DRON-8 with a BSV-29 sharp focus tube with a copper anode and a NaI scintillation detector. The scanning rate was 1°/min with the angle ranging from 5 to 40° (2θ). Origin Pro software (version 2018) was used to analyze the data. For comparison purposes, the crystallinity index was also calculated using the XRD analysis (X_{XRD}) from Equation (2) [30]:

$$X_{XRD} = \frac{Ac}{Ac + Aa} \times 100\% \quad (2)$$

where Ac and Aa are area of crystalline peaks and area of amorphous peaks.

2.3.5. The Porosity of the PHB/PEG Nanofiber Mat

To analyze the porosity of the PHB/PEG nanofiber mat, we cut the sample with a size of 2 × 2 cm and measured the sample weight and the sample thickness. The porosity of the PHB/PEG nanofiber mat was calculated using the following Equation (3) [31]:

$$\text{porosity} = 1 - \frac{\rho 1}{\rho 0} \quad (3)$$

where $\rho 1 = \frac{m1}{h1 \times l1 \times w1}$ is the density of the PHB/PEG nanofiber mat (g/mm^3), $m1$ is the mass of the nanofiber mat (g), $h1$ is the thickness of the PHB nanofiber mat (mm), $l1$ is the length of the nanofiber mat (mm), $w1$ is the width of nanofiber mat (mm), and $\rho 0$ is the average density of two polymers (PHB at 1.19 g·cm^{-3} and PEG at 1.21 g·cm^{-3}).

2.3.6. Mechanical Properties

The mechanical properties of the PHB/PEG nanofiber mat were measured using the Instron 5943 tensile testing machine (Instron, Norwood, MA, USA). The rectangular test sample was cut to size 10 × 1 cm according to ISO 527-3. The sample working range was 8 cm, and the sample pulling speed was 50 mm/min. The thickness of the sample was performed from three points on the sample.

2.3.7. Water Contact Angle Measurement

DSA100 drop-shape analyzer (Kruss, Hamburg, Germany) was used to study the contact angle of the PHB/PEG nanofiber mat. An image of the drop is recorded using a camera and transferred to the drop shape analysis software.

3. Results

3.1. Morphology of Electrospun PHB Fibers

To choose the optimal PHB concentration to mix with PEG, we varied the PHB concentration from 4 to 12% and fixed the electrospinning process specifications as follows: the voltage was set at 30 kV, the distance between the needle tip and collector was 15 cm, the feed rate of the polymer solution was 0.3 mL/h, and there were 18G steel needles. The morphology and distribution of diameter of electrospun PHB fibers are shown in Figure 2.

When the PHB concentration exceeds 8%, the electrospinning process becomes stable, without defects, and the solution drops. The fiber diameter also increases with the increasing PHB concentration; this has been proven in some research [32,33]. However, electrospun fibers are characterized by a high aspect ratio (length to diameter), small pore size, and large surface area. Thus, to achieve these properties, the fiber diameter should be as small as possible; therefore, the concentration of 8% PHB was chosen to make the nanofiber mat with PEG.

Figure 3 shows the average diameter of the obtained fibers. An increase in the concentration of the PHB leads to an increase in the average diameter of the nanofiber while the other parameters remain unchanged. The average diameter of the nanofibers increases from 571 nm to 1156 nm, with an increase in the concentration of PHB from 4% to 12%.

Figure 4 demonstrates the morphology of electrospun PHB/PEG fibers with various concentrations of PEG. When increasing the PEG concentration, the electrospinning process is still stable. No defects or solution drops are detected.

However, with increasing PEG concentration, the diameter of the obtained fiber initially decreased from 1177 nm to 1101 nm, corresponding to 2% PEG, then the diameter of the fiber increased again from 1101 nm to 1136 nm, corresponding to 4% PEG. (Figure 5). This can be explained by the increase in the conductivity of the solution and the surface charge density of the solution jet [34].

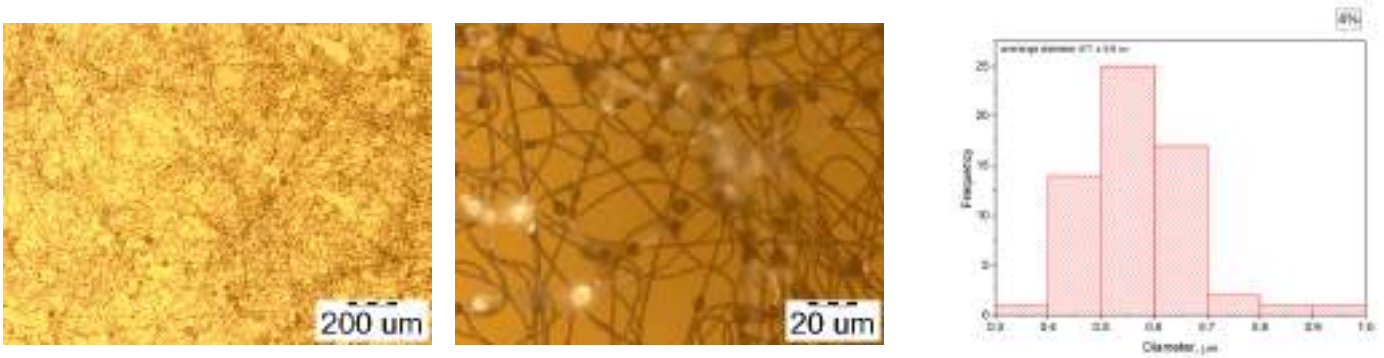

(**a**)

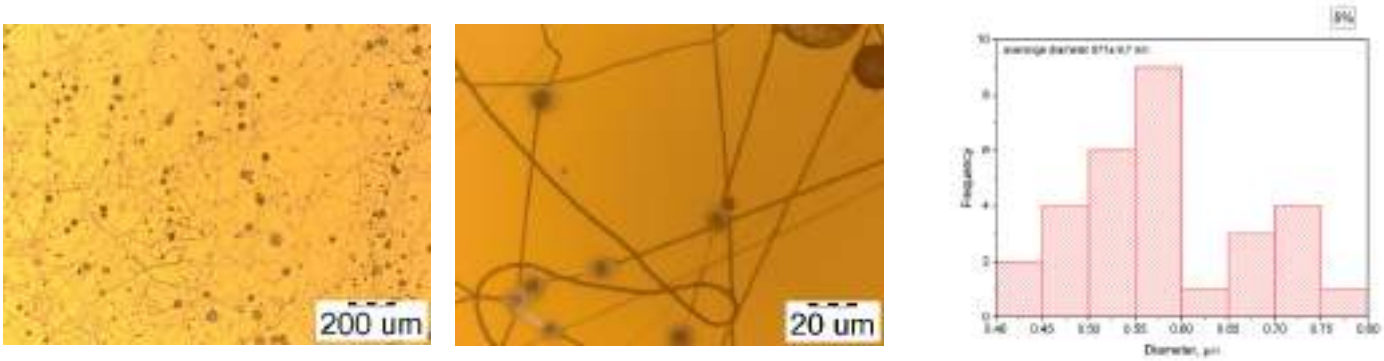

(**b**)

Figure 2. *Cont.*

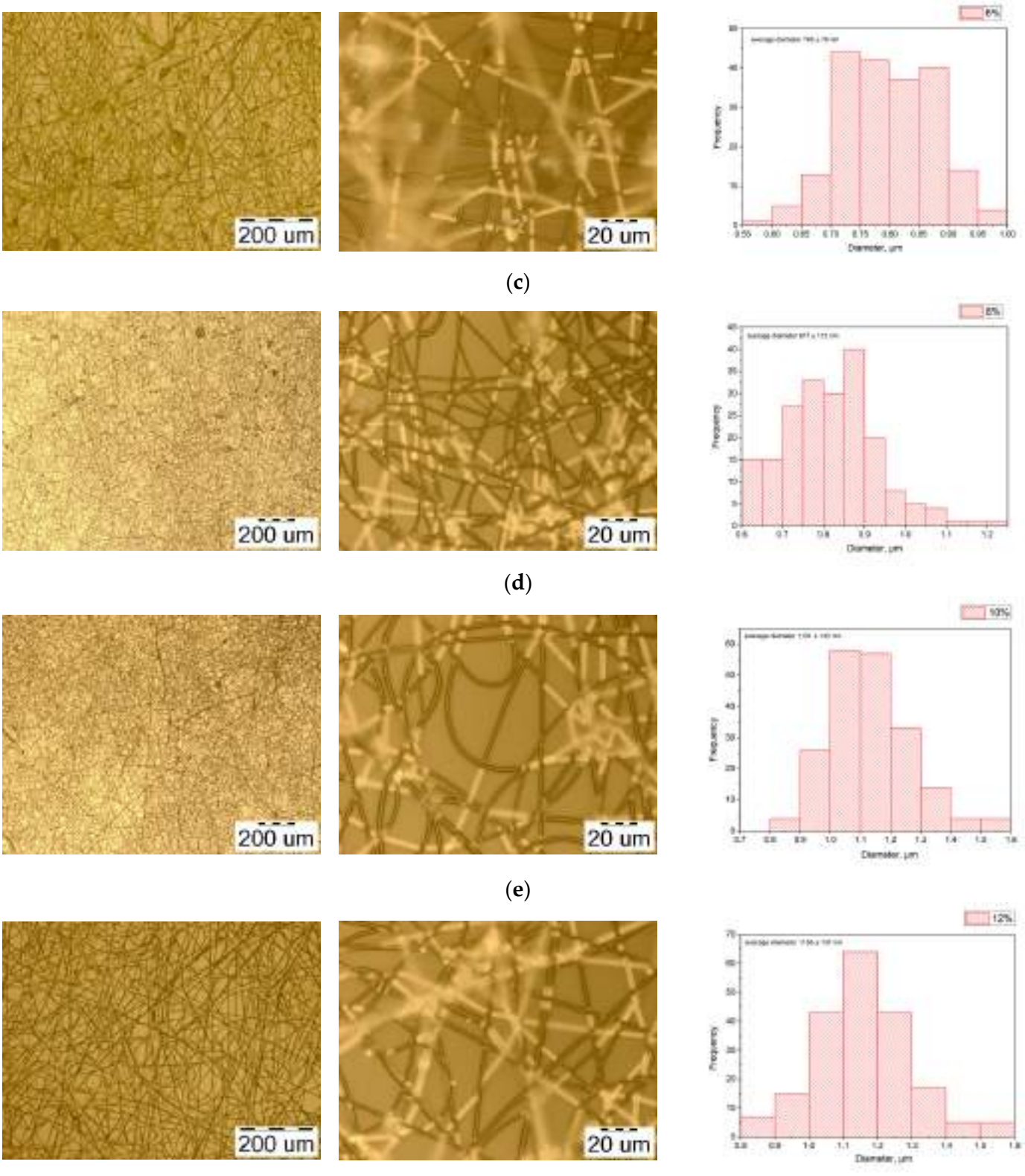

Figure 2. The morphology of electrospun PHB fibers with various concentrations of PHB: (**a**) 4%; (**b**) 5%; (**c**) 6%; (**d**) 8%; (**e**) 10%; (**f**) 12%.

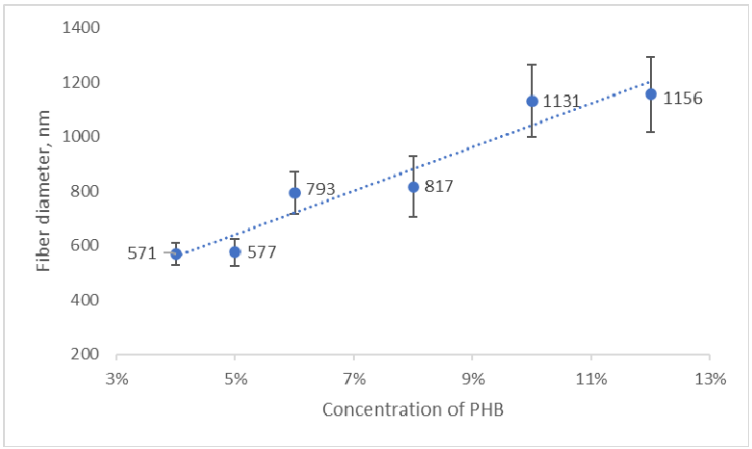

Figure 3. The evolution of the mean fiber diameter with increasing concentrations of PHB.

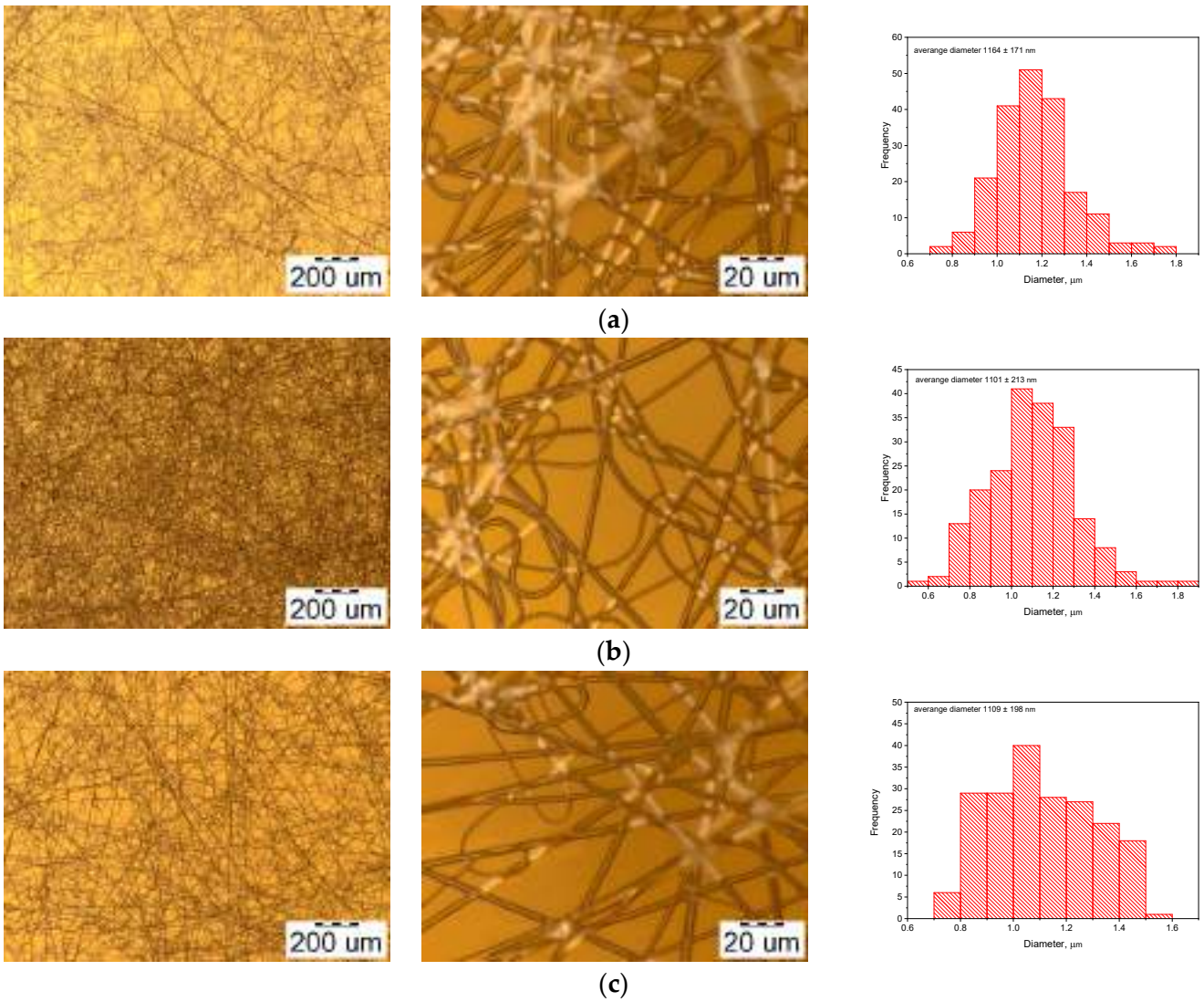

Figure 4. *Cont.*

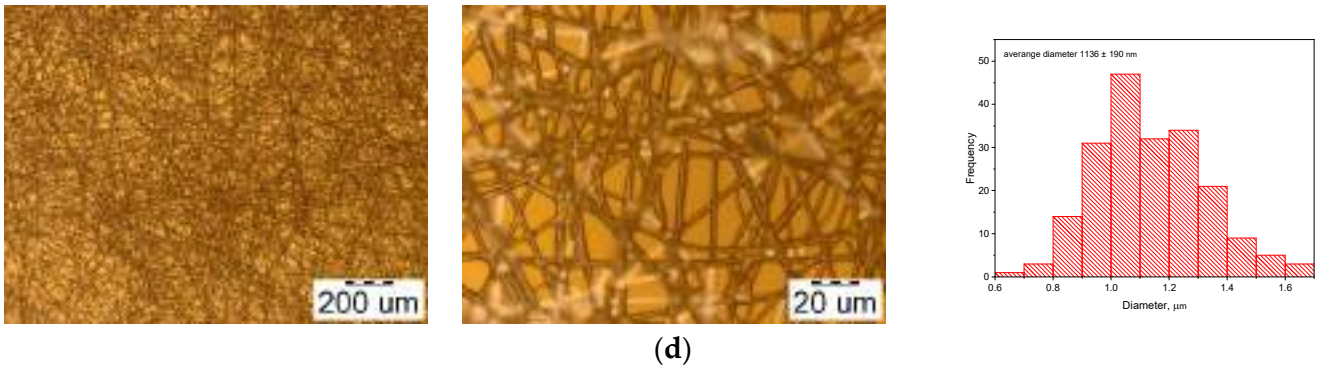

Figure 4. The morphology of electrospun PHB/PEG fibers with various concentrations of PEG: (**a**) 1%; (**b**) 2%; (**c**) 3%; (**d**) 4%.

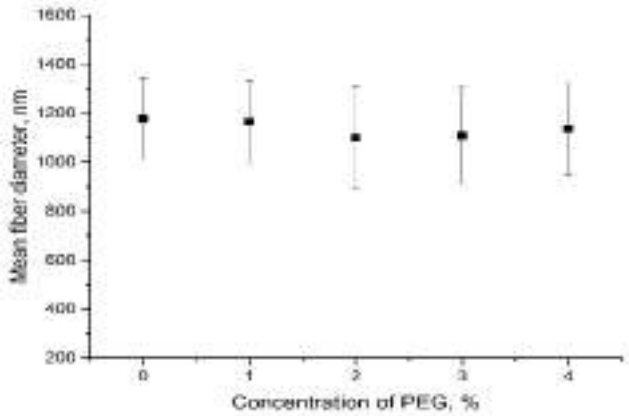

Figure 5. The evolution of the mean fiber diameter with increasing concentrations of PEG.

3.2. Fourier Transform Infrared Spectroscopy (FTIR)

Fourier transform infrared (FTIR) spectra present structural information of material. Figure 6 reveals the spectra in the 600−4000 cm^{-1} range. The FTIR spectrum for PHB nanofibers mat demonstrated the characteristic absorption bands of 1720 cm^{-1}, which corresponded to C=O stretching vibration, and an accompanying band near 2928 cm^{-1} was attributed to the methylene C–H vibration. C–H and ether stretching bands of the PEG pellet were detected at 2870 and 1109 cm^{-1}. Many studies have determined the existence of hydrogen bonds between PHB and PEG molecules. Ol'khov et al. [35], based on DSC data, hypothesized that the terminal hydroxyl groups of PEG macromolecules can form hydrogen bonds with PHB chain units. Accordingly, PEG acts as a bridge between PHB molecules. These authors also claim that the terminal OH group of liquid PEG400 is either associated with each other to form a cyclic hydrogen-bonded structure or reacts with the oxygen atoms of oxyethylene units of adjacent chains. H-bond was also detected in some mixtures of PEG with other polymers, such as PVA/PEG [36] and PVP/PEG [37].

In this work, we can see that, with increasing PEG, the transmittance of the carbonyl group also increases. Therefore, to better determine the effect of PEG on PHB, it seems necessary to further analyze the DSC results and the mechanical properties.

3.3. Thermal Properties

Differential (TGA) and derivative thermogravimetry (DTG) can provide useful information about the thermal stability and degradation of polymer materials. Thermograms of TGA and DTG of the PHB fiber, PEG pellet, and PHB/PEG nanofiber mats with various PEG are demonstrated in Figure 7.

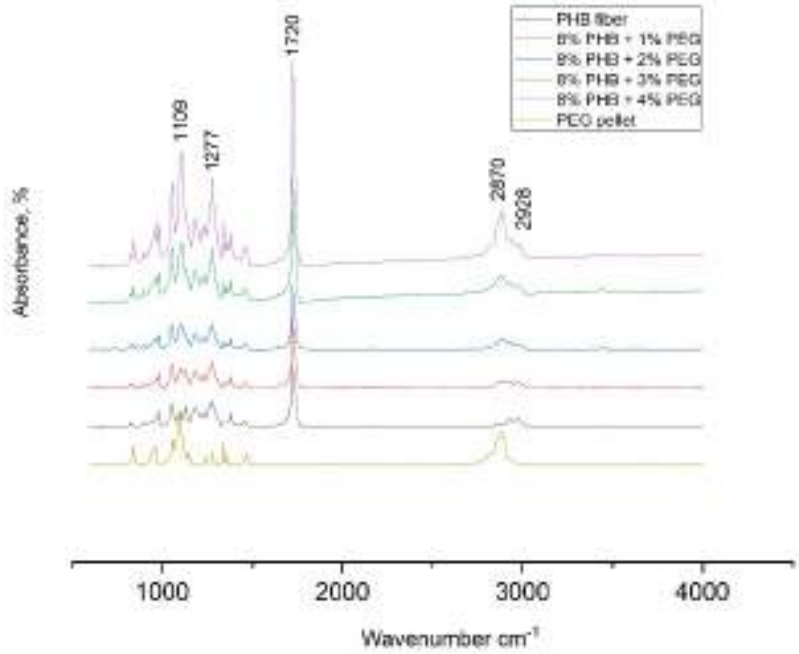

Figure 6. Fourier transform infrared spectroscopy PHB pellet, PEG pellet, PHB/PEG nanofiber mat.

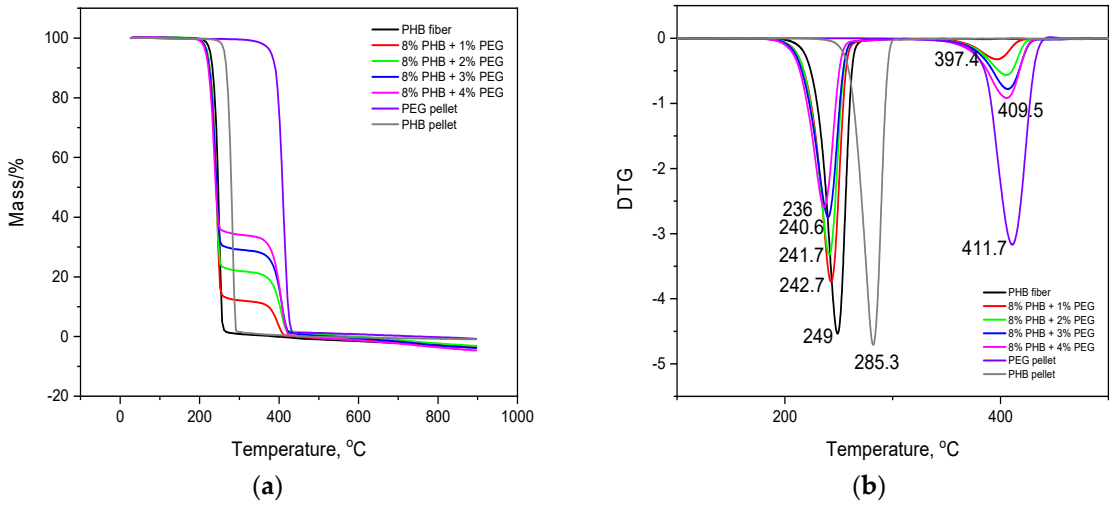

Figure 7. Thermogravimetric analysis (**a**) and difference thermogravimetry (DTG) (**b**) of PHB pellet, PEG pellet, and PHB/PEG nanofiber mat.

The TGA thermogram shows that the degradation process of the PHB nanofiber mat and PHB pellet occurs in one stage. The temperature decomposition of PHB begins at 228 °C and finishes at 270 °C. The temperature decomposition of the PHB nanofiber mat is about 30 °C lower than the PHB pellet, and it could be attributed to the higher specific surface area of the fibrous structures, which was more affected by heating. According to the aforecited authors, as the heating spreads by conduction within the materials, the fibers characterized by a large surface area could reach the degradation temperature faster. Hence, if the surface area seems to be the predominant factor in thermal stabilization, the results presented by TGA were inconclusive with respect to correlating the thermal stability with the two forms of PHB crystallinity [38]. The degradation process of the PEG pellet occurs in one stage. The temperature decomposition begins at 388 °C and finishes at 411 °C.

The TGA thermogram (Figure 7a) of the PHB/PEG nanofiber mat shows two steps of decomposition. Some reports found a mass loss in the temperature range of 30 °C to 100 °C. Atul et al. [39] believed that it is due to the evaporation of chloroform and water

during synthesis that physically adsorbed onto solid PHB/PEG blends sample interlayers. However, in this research, it was not noticed. The first stage of decomposition begins at around 220 °C and finishes at around 240 °C. The second stage of decomposition begins at about 380 °C and finishes at around 410°C. It is also interesting to note that the PHB/PEG nanofiber mat samples showed higher thermal stability than the pure PHB nanofiber mat. According to [40], the incorporation of PEG was found to compromise the thermal stability of PHB through the decreased T_{onset}. This may be due to the hydroxyl group in PEG, which may accelerate the PHB degradation. The decreased trend in the T_{max} related to PHB and PEG phase was mostly observed in PHB blends.

From the DTG curves shown in Figure 7b, the maximum weight loss rates and degradation onset temperatures were obtained for all samples, which are presented in Table 1.

Table 1. TGA and DTG results of PHB pellet, PEG pellet, and PHB/PEG nanofiber mat.

Sample	$T_{onset\,1}$, °C	$T_{d,1}$, °C	Weight Loss Rate, %/°C	$T_{onset\,2}$, °C	$T_{d,2}$, °C	Weight Loss Rate, %/°C
PHB pellet	265.3	285.3	6.1			
PHB fiber (8%)	228.9	251.4	5.6			
PHB 8% + PEG 1%	224.3	244.7	4.5	377.0	396.6	0.3
PHB 8% + PEG 2%	224.2	243.3	4.0	381.7	408.6	0.6
PHB 8% + PEG 3%	222.3	241.8	3.1	383.0	408.7	0.8
PHB 8% + PEG 4%	219.8	237.3	3.0	381.9	409.5	1.0
PEG pellet	-	-	-	388.8	411.7	3.5

It was observed that the weight loss rate decreased from 4.5% to 3.0% with the increase in PEG loading during the first stage of decomposition. In the second stage of decomposition, the weight loss rate increased from 0.3% to 1% with the increase in PEG loading. The addition of PEG to the blends formed H-bonds with PHB segments, causing a decrease in the weight loss rate, the same as in PVA/PEG [36] and PVP/PEG mixtures [37].

3.4. Differential Scanning Calorimetry (DSC) Analysis

Figure 8 and Table 2 demonstrate the results of the DSC analysis. The fabrication of PHB fibers affects the crystallization and the crystallinity of PHB—the degree of crystallinity decreases by 10%. This decrease is also credited to Parra et al. [41]. Zhao et al. [42] showed that increasing the voltage increases the bonding of polymer chains, thereby increasing the crystallinity. However, the crystallinity is also affected by the distance between the needle and the collector. This increase in the degree of crystallinity with an increase in electrospinning voltage is not expected to continue indefinitely. On the contrary, above a voltage (the optimum electrospinning voltage), the degree of crystallinity will reduce. This is because the degree of crystallinity is also influenced by the flight time of the jet, which at high voltages is short enough to leave insufficient time for the polymer to crystallize [43]. Increasing PEG content did not change the crystallinity of PHB in the nanofiber mats, and the crystallinity remains at about 27%. The crystallinity of PEG in the nanofiber mats is reduced compared to that of the PEG pellet, which is caused by the formation of H-bonding between PEG and PHB in the PHB/PEG nanofiber mat, which hindered the crystallization step. However, as PEG content grows, the crystallinity of PEG in the nanofiber mats also increases because with the increase in the PEG content, a part of the PEG molecule that does not participate in H-bond with PHB links together by intramolecular hydrogen bonds [44] to form large PEG molecular clusters leading to the increased crystallinity of PEG in the nanofiber mats.

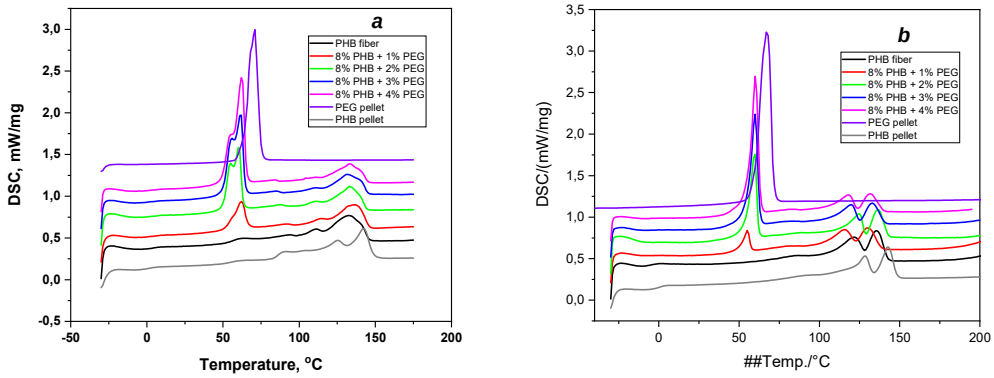

(**a**) (**b**)

Figure 8. DSC thermograms for PHB pellet, PEG pellet, and PHB/PEG nanofiber mat at different PEG loadings: (**a**) first heating and (**b**) second heating.

Table 2. DSC data (first and second heating curves) of PHB pellet, PEG pellet, and PHB/PEG nanofiber mat.

Sample	T_g, °C	$T_{m,PEG}$, °C		$\Delta H_{m,PEG}$, J/g	$T_{m,PHB}$, °C		$\Delta H_{m,PHB}$, J/g	X_{DSC}, %	
								PEG	PHB
First heating									
PHB pellet	1.4	-		-	125.4	142.3	56.0	-	38.3
PHB fiber (8%)	3.8	-		-	110.8	133.0	39.0	-	26.7
PHB (8%) + PEG (1%)	−1.0	-	62.2	17.0	115.1	136.3	35.1	72.4	27.1
PHB (8%) + PEG (2%)	−0.1	55.1	60.4	38.4	112.2	133.0	31.5	90.8	26.9
PHB (8%) + PEG (3%)	−1.1	55.7	61.6	53.0	111.0	131.5	29.1	92.0	27.4
PHB (8%) + PEG (4%)	3.5	55.5	62.3	65.0	112.8	133.0	26.2	92.2	26.9
PEG pellet	-		70.5	211.4	-	-		100	-
Second heating									
Pellet PHB	0.1	-	-	-	128.4	142.5	43.5	-	29.8
PHB fiber (8%)	−2.7	-	-	-	121.7	135.3	44.1	-	28.2
PHB (8%)/PEG (1%)	−5.0	53.8	60.4	8.0	121.8	134.7	34.4	33.9	29.9
PHB (8%)/PEG (2%)	−3.9	54.3	61.8	35.5	124.6	136.7	34.3	83.9	28.4
PHB (8%)/PEG (3%)	−3.1	54.8	61.9	49.3	119.7	133.0	30.4	85.5	28.5
PHB (8%)/PEG (4%)	−1.3	55.5	62.7	60.4	118.1	131.8	27.0	85.7	28.5
Pellet PEG	-		67.3	200.7			-	100	-

The endothermic peaks at the temperature of 62 °C and at the temperatures of 110–140 °C are characteristics of the PEG melting in PHB/PEG nanofiber mat and the melting of PHB in PHB/PEG nanofiber mat, respectively. PHB has two endothermic melting peaks corresponding to the melting of PHB crystals formed from recrystallization during the heating cycle. It was also researched by Susan et al. [10], where multiple melting peaks were observed for each PHB incorporated with a plasticizer (PEG).

The melting temperature of PEG in the PHB/PEG nanofiber mat (Tm PEG) decreased when adding PEG into PHB/PEG nanofiber mat compared with PEG pellets. A little difference in Tm PEG values was observed for PHB/PEG nanofiber mat at all various PEG loadings. Similar to PEG, the melting temperature of PHB in PHB/PEG nanofiber mat (Tm PHB) decreased from 125 °C to 110–115 °C when adding PEG. Mixing PEG with PHB has no effect on the melting temperature of the PHB/PEG nanofiber mats, and the melting temperature remains about 110–115 °C. The glass transition temperature (Tg) of the PHB/PEG nanofiber mat changes irregularly.

The cooling curves shown in Figure 9 for the PHB/PEG nanofiber mat demonstrate two or three main crystallization events related to PEG and PHB crystallization temperatures. The crystallization temperatures of the PEG pellet are 42.6 °C and PHB 89.8 °C.

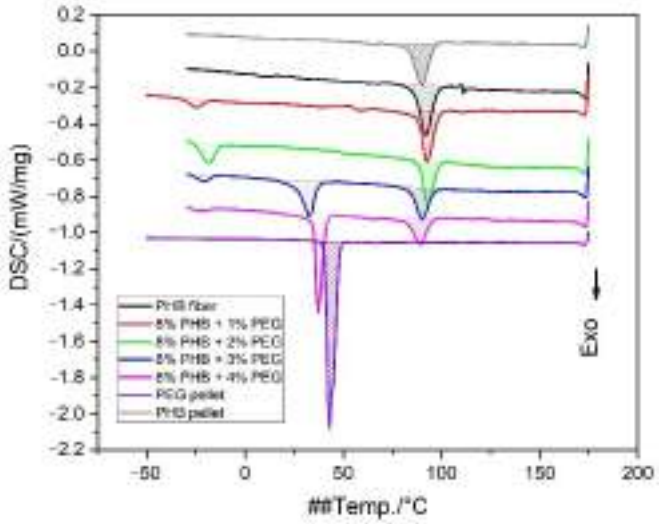

Figure 9. DSC thermograms (cooling curves) for PHB pellet, PEG pellet, and PHB/PEG nanofiber mat.

The presence of PEG has little effect on the crystallization temperature of PHB (see Table 3). However, PEG itself crystallizes in a mixture with PHB at significantly lower temperatures. Several peaks of PEG crystallization are observed when the PHB concentration increases, which may be due to incompatibility in mixtures containing a high PEG concentration.

Table 3. DSC data (cooling curves) of PHB pellet, PEG pellet, and PHB/PEG nanofiber mat.

Sample Code	$T_{c,PEG}$, °C	$\Delta H_{c,PEG}$, J/g	$T_{c,PHB}$, °C	$\Delta H_{c,PHB}$, J/g
Pellet PHB	-	-	89.8	40.1
PHB (8%)	-	-	92.2	44.6
PHB (8%)/PEG (1%)	−24.7	7.4	92.9	44.7
PHB (8%)/PEG (2%)	−19.1	16.2	93.0	32.1
PHB (8%)/PEG (3%)	−21.6 32.2	5.4 28.7	90.2	28.3
PHB (8%)/PEG (4%)	−21.6 37.0	2.7 44.0	88.8	23.3
Pellet PEG	42.6	196.7	-	-

3.5. Crystalline Structure

X-ray diffraction (XRD) patterns of the PHB/PEG nanofiber mats are shown in Figure 10. As seen in Figure 10, all samples presented two strong crystalline peaks at $2\theta \approx 13.5°$ and 17°, which corresponded to the (020) plane and (110) plane of the orthorhombic unit cell of the PHB [30,45]. When adding PEG, two more peaks appear at $2\theta \approx 19°$ and $2\theta \approx 23°$, which correspond to the PEG [45].

As seen in Table 4, along with the increase in PEG content, the X_{XRD} values (%) obtained from the XRD spectrum initially decreased and then increased, while the X_{DSC} values were almost unchanged. The difference between the crystallinities reported by DSC and XRD can be associated with the difference between the methods; XRD emphasizes surface crystallinity, while DSC represents bulk behavior [30].

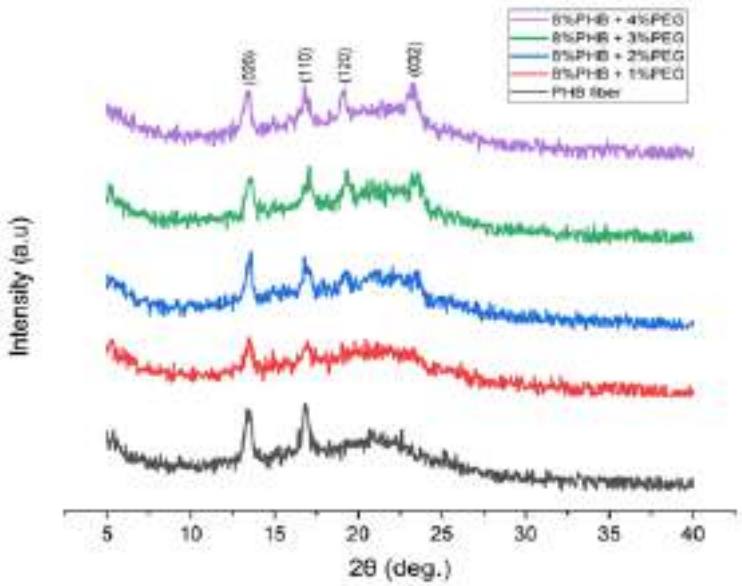

Figure 10. XRD patterns of the PHB/PEG nanofiber mats.

Table 4. The degree of crystallinity of PHB/PEG nanofiber mats by XRD and DSC method.

Sample Code	X_{XRD}, %	X_{DSC}, %
PHB (8%)	28.9	26.7
PHB (8%)/PEG (1%)	17.5	27.1
PHB (8%)/PEG (2%)	18.1	26.9
PHB (8%)/PEG (3%)	26.8	27.4
PHB (8%)/PEG (4%)	29.0	26.9

3.6. The Porosity of the PHB/PEG Nanofiber Mat

Table 5 shows the porosity of the PHB/PEG nanofiber mat. First, the porosity of the PHB/PEG nanofiber mat increases in comparison with the PHB nanofiber mat. With the increase in PEG concentration, the porosity also increases. Karina et al. [46] showed that larger fiber diameters provide lower porosity and larger pore size. This increase has also been confirmed in several studies. Heyun et al. [47] showed that with the irregular change in the fiber diameter of the PU/PEG nanofiber mats, the porosity also increased. However, Elena et al. [48] showed that when the concentration of PEG was increased in PLA/PEG nanofiber mats, the fiber diameters increased with decreased porosity.

Table 5. The porosity of PHB fiber and PHB/PEG nanofiber mat.

Sample Code	Average Density, g/cm^3	Porosity, %
PHB (8%)	1.190	62.91
PHB (8%)/PEG (1%)	1.192	63.95
PHB (8%)/PEG (2%)	1.194	55.73
PHB (8%)/PEG (3%)	1.195	70.24
PHB (8%)/PEG (4%)	1.197	70.33

3.7. The Mechanical Properties of the PHB/PEG Nanofiber Mat

The sample for mechanical testing tensile, typical stress–strain diagram, and strength test result of the PHB/PEG nanofiber mat are demonstrated in Figure 11 and Table 6. Tensile strength increased from 3.6 ± 0.2 MPa to a maximum of 4.4 ± 0.8 MPa corresponding to 2 wt% of PEG concentration, and then decreased with the increased PEG concentration to 4%. Elongation at break decreased from 58 ± 21% to 3 ± 1% with the increased PEG concentration.

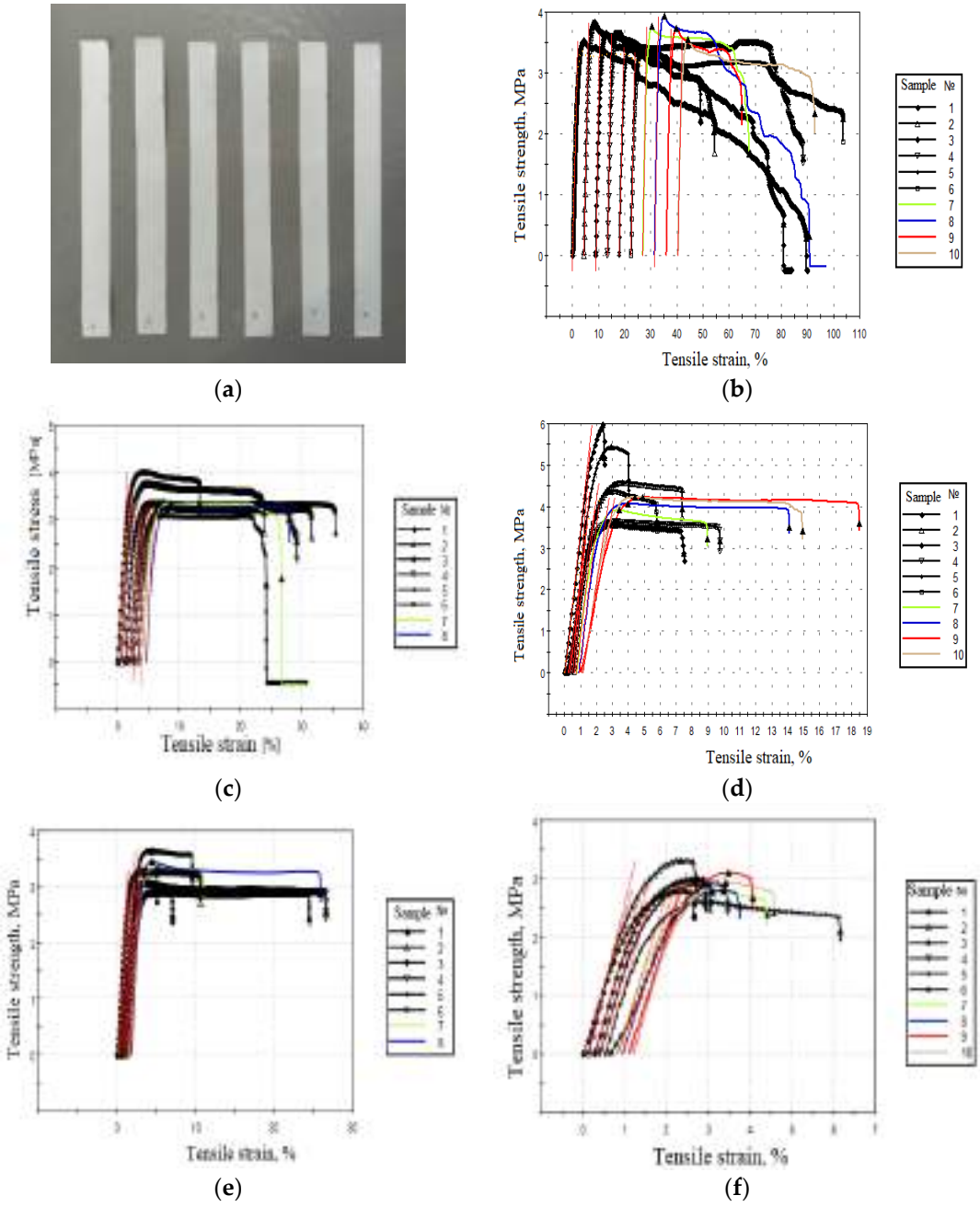

Figure 11. A sample for mechanical testing (**a**) and PHB/PEG nanofiber mat stress–strain diagrams with a 0% (**b**), 1% (**c**), 2% (**d**), 3% (**e**), and 4% (**f**) concentrations of PEG.

Table 6. The mechanical properties of PHB fiber and PHB/PEG nanofiber mat.

Sample Code	Tensile Strength (σ), MPa	Young's Modulus, E (MPa)	Elongation at Break (%)
PHB (8%)	3.6 ± 0.2	232.3 ± 28.7	58 ± 21
PHB (8%)/PEG (1%)	3.4 ± 0.3	254.4 ± 26.7	24 ± 6
PHB (8%)/PEG (2%)	4.4 ± 0.8	332.2 ± 89.3	9 ± 5
PHB (8%)/PEG (3%)	3.2 ± 0.3	267.7 ± 33.8	14 ± 9
PHB (8%)/PEG (4%)	2.9 ± 0.2	242.3 ± 29.4	3 ± 1

Shirin et al. [49] claimed that blending the PPSU solution with 2 and 5 wt% PEG reduced both elastic modulus and tensile strength, whereas the elongation at break was

increased. The reason is that adding PEG as a plasticizer facilitates the movement of polymeric chains and reduces the brittleness of the prepared nanofiber mats. However, a further increase in PEG concentration to 10 wt% contributed to a dramatic increase in the tensile properties because of the inter-fiber bonding formation in the nanofiber mats. Moreover, Parra et al. [20] showed that tensile strength was reduced by the addition of PEG. These results indicated that the plasticizer reduced any restraint imposed on the separation of the lamellae during the mechanical test. PEG probably inhibited the relative chain motion or reduced the force of secondary intermolecular bonds between the PHB chains. This is consistent with the assumption we made above, where a part of the PEG molecule that does not participate in H-bond with PHB links together by intramolecular hydrogen bonds to form large PEG molecular clusters leading to increased crystallinity of PEG in PHB/PEG nanofiber mat.

3.8. Water Contact Angle

The hydrophobic property of the PHB/PEG nanofiber mat is characterized by the contact angle of the nanofiber mat with the water droplet on the surface of the nanofiber mat. The water contact angle of the PHB nanofiber mat was 127°, which is 10° lower than in some other studies [38,50]. This value shows that the PHB nanofiber mat has a hydrophobicity, and the PHB nanofiber mat cannot be used for water purification because of the nanofiber mat's hydrophobicity. The contact angle image of the PHB nanofiber mat and PHB/PEG nanofiber mats at the initial time is shown in Figure 12.

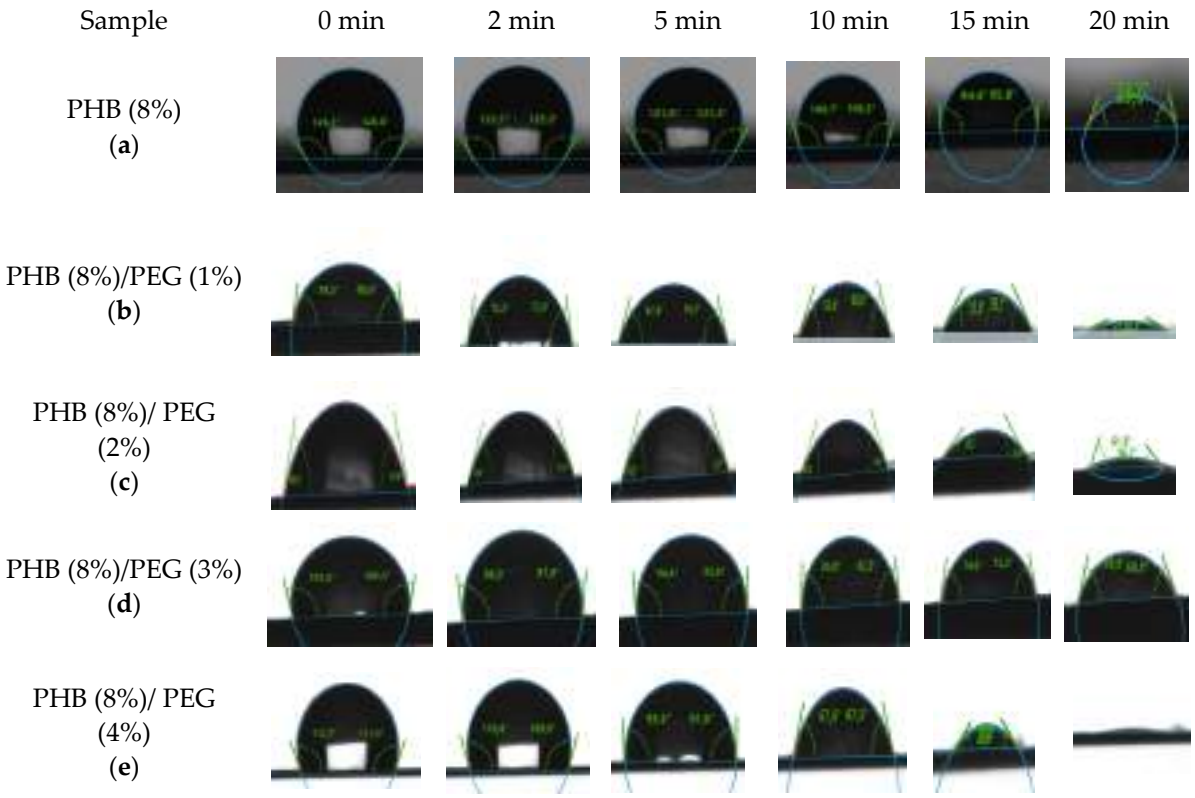

Figure 12. The contact angle image of the PHB nanofiber mat (**a**) and PHB/PEG nanofiber mats with 0% (**a**), 1% (**b**), 2% (**c**), 3% (**d**), 4% (**e**) with the time.

Figure 13 shows the change in contact angle with the time of the PHB/PEG nanofiber mat. The contact angle was measured after 0, 2, 5, 10, 15, and 20 min of water being dropped on the nanofiber mat surface; the contact angle was significantly reduced, and after about 20 min, the water droplets completely penetrated the nanofiber mat surface. This phenomenon occurs due to the PEG dissolution by water.

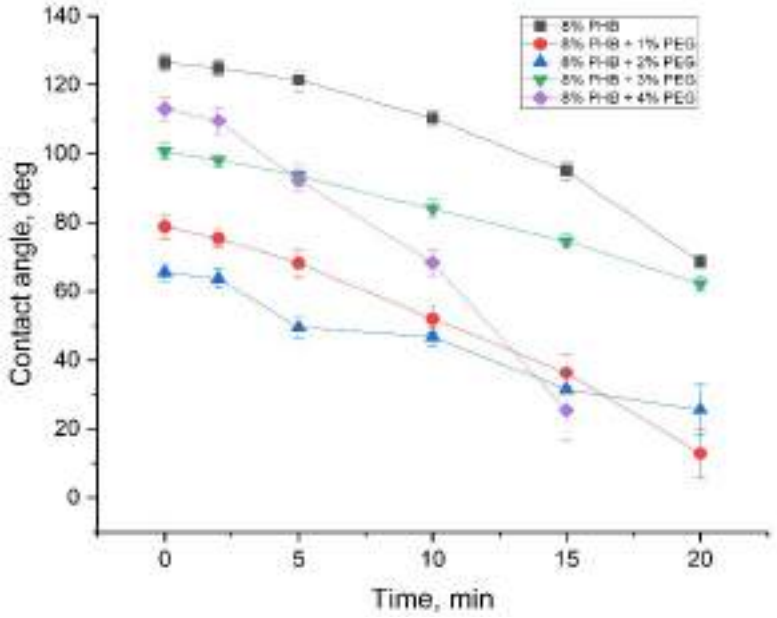

Figure 13. The change in contact angle with the time of PHB/PEG nanofiber mat.

4. Conclusions

In this research, the effect of PHB concentration on the morphology of nanofibers was studied by changing the PHB concentration from 4 to 12%; the results showed that when the concentration of PHB increased, the diameter of the fiber also increased. The concentration of 8% PHB was selected based on the criteria of fibers with minor defects and the minimum average diameter. Then the PHB content was fixed at 8% and added PEG with a 1 to 4% concentration. The results of the PHB/PEG nanofiber morphology study showed that initially, the fiber diameter decreased, then increased again. Then the electrospinning method successfully obtained the PHB/PEG nanofiber mat with various PEG concentrations loading. The characteristic of the PHB/PEG nanofiber mat was analyzed by a microscope, FTIR, thermal properties, and mechanical properties methods. The results showed that adding PEG improved the hydrophobicity, porosity, and thermal stability of the PHB nanofiber mat. The porosity of the PHB/PEG nanofiber mat increases when the increase in PEG concentration. Tensile strength increased, reaching a maximum of 2 wt% of PEG concentration, then decreased with the increased PEG concentration. The water contact angle was decreased when mixing PEG, which showed that PHB/PEG nanofiber mats have great potential for water purification applications. However, increasing PEG concentration leads to the formation of Intramolecular hydrogen bonds between PEG molecules, which increases the crystallinity of PEG in PHB/PEG nanofiber mats, leading to a decrease in the mechanical properties of the nanofiber mats.

Author Contributions: Conceptualization, M.U. and R.O.; formal analysis, N.H.T., V.S., A.K. and R.O.; investigation, N.H.T. and R.O.; resources, N.H.T. and R.O.; writing—original draft preparation, N.H.T. and R.O.; writing—review and editing, N.H.T., R.O, P.S., V.S. and M.U.; visualization, N.H.T., R.O. and M.U.; supervision, R.O. and M.U.; project administration, M.U.; funding acquisition, M.U. All authors have read and agreed to the published version of the manuscript.

Funding: This research received no external funding.

Institutional Review Board Statement: Not applicable.

Informed Consent Statement: Not applicable.

Data Availability Statement: Not applicable.

Conflicts of Interest: The authors declare no conflict of interest.

References

1. Leena, M.M.; Yoha, K.S.; Moses, J.A.; Anandharamakrishnan, C. Nanofibers in Food Applications. In *Innovative Food Processing Technologies: A Comprehensive Review*; Elsevier: Amsterdam, The Netherlands, 2021; pp. 634–650. [CrossRef]
2. Nunes, C.S.; Philipps-Wiemann, P. Formulation of enzymes. In *Enzymes in Human and Animal Nutrition*; Academic Press: London, UK, 2018; pp. 429–440. [CrossRef]
3. Alghoraibi, I.; Alomari, S. Different Methods for Nanofiber Design and Fabrication. In *Handbook of Nanofibers*; Springer International Publishing: Cham, Switzerland, 2018; pp. 1–46. [CrossRef]
4. Zhao, Y.; Qiu, Y.; Wang, H.; Chen, Y.; Jin, S.; Chen, S. Preparation of Nanofibers with Renewable Polymers and Their Application in Wound Dressing. *Int. J. Polym. Sci.* **2016**, *2016*, 4672839. [CrossRef]
5. Sundarrajan, S.; Tan, K.L.; Lim, S.H.; Ramakrishna, S. Electrospun nanofibers for air filtration applications. *Procedia Eng.* **2014**, *75*, 159–163. [CrossRef]
6. Maliszewska, I.; Czapka, T. Electrospun Polymer Nanofibers with Antimicrobial Activity. *Polymers* **2022**, *14*, 1661. [CrossRef]
7. Ma, W.; Zhang, Q.; Hua, D.; Xiong, R.; Zhao, J.; Rao, W.; Huang, S.; Zhan, X.; Chen, F.; Huang, C. Electrospun fibers for oil-water separation. *RSC Adv.* **2016**, *6*, 12868–12884. [CrossRef]
8. Yoo, H.S.; Kim, T.G.; Park, T.G. Surface-functionalized electrospun nanofibers for tissue engineering and drug delivery. *Adv. Drug Deliv. Rev.* **2009**, *61*, 1033–1042. [CrossRef]
9. Deng, Z.; Mu, H.; Jiang, L.; Xi, W.; Xu, X.; Zheng, W. Preparation and characterization of electrospun PLGA-SF nanofibers as a potential drug delivery system. *Mater. Chem. Phys.* **2022**, *289*, 126452. [CrossRef]
10. Yang, X.; Chen, Y.; Zhang, C.; Duan, G.; Jiang, S. Electrospun carbon nanofibers and their reinforced composites: Preparation, modification, applications, and perspectives. *Compos. Part B Eng.* **2023**, *249*, 110386. [CrossRef]
11. Guo, Y.; Qiao, Y.; Cui, T.; Wu, F.; Ji, S.; Yang, Y.; Tian, H.; Ren, T. Electrospun Nanofibers for Integrated Sensing, Storage, and Computing Applications. *Appl. Sci.* **2022**, *12*, 4370. [CrossRef]
12. Li, M.; Qiu, W.; Wang, Q.; Li, N.; Liu, L.; Wang, X.; Yu, J.; Li, X.; Li, F.; Wu, D. Nitric Oxide-Releasing Tryptophan-Based Poly(ester urea)s Electrospun Composite Nanofiber Mats with Antibacterial and Antibiofilm Activities for Infected Wound Healing. *ACS Appl. Mater. Interfaces* **2022**, *14*, 15911–15926. [CrossRef]
13. Qi, Y.; Wang, C.; Wang, Q.; Zhou, F.; Li, T.; Wang, B.; Su, W.; Shang, D.; Wu, S. A simple, quick, and cost-effective strategy to fabricate polycaprolactone/silk fibroin nanofiber yarns for biotextile-based tissue scaffold application. *Eur. Polym. J.* **2023**, *186*, 111863. [CrossRef]
14. Choy, S.; Moon, H.; Park, Y.; Jung, Y.M.; Koo, J.M.; Oh, D.X.; Hwang, D.S. Mechanical properties and thermal stability of intermolecular-fitted poly(vinyl alcohol)/α-chitin nanofibrous mat. *Carbohydr. Polym.* **2020**, *244*, 116476. [CrossRef]
15. Zhu, M.; Han, J.; Wang, F.; Shao, W.; Xiong, R.; Zhang, Q.; Pan, H.; Yang, Y.; Samal, S.K.; Zhang, F.; et al. Electrospun Nanofibers Membranes for Effective Air Filtration. *Macromol. Mater. Eng.* **2017**, *302*, 1600353. [CrossRef]
16. Lee, S.J.; Oh, S.H.; Liu, J.; Soker, S.; Atala, A.; Yoo, J.J. The use of thermal treatments to enhance the mechanical properties of electrospun poly(ε-caprolactone) scaffolds. *Biomaterials* **2008**, *29*, 1422–1430. [CrossRef]
17. Wang, W.; Jin, X.; Zhu, Y.; Zhu, C.; Yang, J.; Wang, H.; Lin, T. Effect of vapor-phase glutaraldehyde crosslinking on electrospun starch fibers. *Carbohydr. Polym.* **2016**, *140*, 356–361. [CrossRef]
18. Mas, A.; Jaaba, H.; Sledz, J.; Schue, F. Membranes en PHB, P(HB-co-9% HV), P(HB-co-22% HV) pour la microfiltration ou la pervaporation proprietes filtrantes et etat de surface. *Eur. Polym. J.* **1996**, *32*, 435–450. [CrossRef]
19. Marova, I.; Kundrat, V.; Benesova, P.; Matouskova, P.; Obruca, S. Use of biodegradable PHA-based nanofibers to removing microorganisms from water. In Proceedings of the 2015 IEEE 15th International Conference on Nanotechnology (IEEE-NANO), Rome, Italy, 27–30 July 2015; pp. 204–206. [CrossRef]
20. Parra, D.F.; Fusaro, J.; Gaboardi, F.; Rosa, D.S. Influence of poly (ethylene glycol) on the thermal, mechanical, morphological, physical-chemical and biodegradation properties of poly (3-hydroxybutyrate). *Polym. Degrad. Stab.* **2006**, *91*, 1954–1959. [CrossRef]
21. Tomietto, P.; Loulergue, P.; Paugam, L.; Audic, J.L. Biobased polyhydroxyalkanoate (PHA) membranes: Structure/performances relationship. *Sep. Purif. Technol.* **2020**, *252*, 117419. [CrossRef]
22. Chan, R.T.H.; Marçal, H.; Russell, R.A.; Holden, P.J.; Foster, L.J.R. Application of polyethylene glycol to promote cellular biocompatibility of polyhydroxybutyrate films. *Int. J. Polym. Sci.* **2011**, *2011*, 473045. [CrossRef]
23. Pham, L.Q.; Uspenskaya, M.V.; Olekhnovich, R.O.; Baranov, M.A. The Mechanical Properties of PVC Nanofiber Mats Obtained by Electrospinning. *Fibers* **2021**, *9*, 2. [CrossRef]
24. Vu, T.H.N.; Morozkina, S.N.; Uspenskaya, M.V. Study of the Nanofibers Fabrication Conditions from the Mixture of Poly(vinyl alcohol) and Chitosan by Electrospinning Method. *Polymers* **2022**, *14*, 811. [CrossRef]
25. Jia, S.; Yu, D.; Zhu, Y.; Wang, Z.; Chen, L.; Fu, L. Morphology, crystallization and thermal behaviors of PLA-based composites: Wonderful effects of hybrid GO/PEG via dynamic impregnating. *Polymers* **2017**, *9*, 528. [CrossRef]
26. Singh, T.J.; Bhat, S. V Morphology and conductivity studies of a new solid polymer electrolyte: (PEG) × LiClO 4. *Bull. Mater. Sci* **2003**, *26*, 707–714. [CrossRef]
27. Nagahama, K.; Aoki, R.; Saito, T.; Ouchi, T.; Ohya, Y.; Yui, N.; Yui, N. Enhanced stereocomplex formation of enantiomeric polylactides grafted on a polyrotaxane platform. *Polym. Chem.* **2013**, *4*, 1769–1773. [CrossRef]

28. Barham, P.J.; Keller, A.; Otun, E.L.; Holmes, P.A. Crystallization and morphology of a bacterial thermoplastic: Poly-3-hydroxybutyrate. *J. Mater. Sci.* **1984**, *19*, 2781–2794. [CrossRef]
29. Wei, L.; McDonald, A.G. Peroxide induced cross-linking by reactive melt processing of two biopolyesters: Poly(3-hydroxybutyrate) and poly(l -lactic acid) to improve their melting processability. *J. Appl. Polym. Sci.* **2015**, *132*, 13. [CrossRef]
30. Bikiaris, D.; Fombuena Borràs, V.; Fernando, M.; Carrasco, A.; Karpova, S.G.; Varyan, I.A.; Olkhov, A.A.; Popov, A.A. A Feature of the Crystalline and Amorphous Structure of Ultra Thin Fibers Based on Poly(3-hydroxybutyrate) (PHB) Containing Minor Concentrations of Hemin and a Complex of Tetraphenylporphyrin with Iron. *Polymers* **2022**, *14*, 4055. [CrossRef]
31. Wang, Z.; Sahadevan, R.; Crandall, C.; Menkhaus, T.J.; Fong, H. Hot-pressed PAN/PVDF hybrid electrospun nanofiber membranes for ultrafiltration. *J. Membr. Sci.* **2020**, *611*, 118327. [CrossRef]
32. Ramakrishna, S.; Fujihara, K.; Teo, W.E.; Lim, T.C.; Ma, Z. *An Introduction to Electrospinning and Nanofibers*; World Scientific Publishing Co.: Singapore, 2005; pp. 1–382. [CrossRef]
33. Bae, H.S.; Haider, A.; Selim, K.M.K.; Kang, D.Y.; Kim, E.J.; Kang, I.K. Fabrication of highly porous PMMA electrospun fibers and their application in the removal of phenol and iodine. *J. Polym. Res.* **2013**, *20*, 158. [CrossRef]
34. Zhao, Y.; Zhu, J.; Zhang, J.; Chen, Z.; Li, W.; Deng, L.; Chen, K.; Wan, H.; Li, J.; Li, R. Optimization of biodegradable PEG/PLGA nanofiber mats electrospinning process for anti-adhesion application. *J. Appl. Polym. Sci.* **2018**, *135*, 46282. [CrossRef]
35. Ol'khov, A.A.; Gol'dshtrakh, M.A.; Ishchenko, A.A.; Iordanskii, A.L. Formation of complexes in polyhydroxybutyrate–polyethylene glycol mixtures. *Russ. J. Phys. Chem. B* **2015**, *9*, 961–970. [CrossRef]
36. Falqi, F.H.; Bin-Dahman, O.A.; Hussain, M.; Al-Harthi, M.A. Preparation of Miscible PVA/PEG Blends and Effect of Graphene Concentration on Thermal, Crystallization, Morphological, and Mechanical Properties of PVA/PEG (10wt%) Blend. *Int. J. Polym. Sci.* **2018**, *2018*, 8527693. [CrossRef]
37. Feldstein, M.M.; Roos, A.; Chevallier, C.; Creton, C.; Dormidontova, E.E. Relation of glass transition temperature to the hydrogen bonding degree and energy in poly(N-vinyl pyrrolidone) blends with hydroxyl-containing plasticizers: 3. Analysis of two glass transition temperatures featured for PVP solutions in liquid poly(ethylene glycol). *Polymer* **2003**, *44*, 1819–1834. [CrossRef]
38. Mottina, A.C. What Changes in Poly(3-Hydroxybutyrate) (PHB) When Processed as Electrospun Nanofibers or Thermo-Compression Molded Film? *Mater. Res.* **2016**, *19*, 57–66. [CrossRef]
39. Tiwari, A.; Hihara, L.H. Thermal stability and thermokinetics studies on silicone ceramer coatings: Part 1—Inert atmosphere parameters. *Polym. Degrad. Stab.* **2009**, *94*, 1754–1771. [CrossRef]
40. Abdallah, H.; El-Gendi, A. Preparation of Polyvinylchloride (PVC) Membranes, Characterization, Modification, Applications, and Mathematical Model. In *Polyvinylchloride-Based Blends: Preparation, Characterization and Applications*; Springer: Cham, Switzerland, 2022; pp. 175–210. [CrossRef]
41. Parra, D.F.; Rosa, D.S.; Rezende, J.; Ponce, P.; Lugão, A.B. Biodegradation of γ Irradiated Poly 3-hydroxybutyrate (PHB) Films Blended with Poly(Ethyleneglycol). *J. Polym. Environ.* **2011**, *19*, 918–925. [CrossRef]
42. Zhao, S.; Wu, X.; Wang, L.; Huang, Y. Electrospinning of ethyl–cyanoethyl cellulose/tetrahydrofuran solutions. *J. Appl. Polym. Sci.* **2004**, *91*, 242–246. [CrossRef]
43. Jarusuwannapoom, T.; Hongrojjanawiwat, W.; Jitjaicham, S.; Wannatong, L.; Nithitanakul, M.; Pattamaprom, C.; Koombhongse, P.; Rangkupan, R.; Supaphol, P. Effect of solvents on electro-spinnability of polystyrene solutions and morphological appearance of resulting electrospun polystyrene fibers. *Eur. Polym. J.* **2005**, *41*, 409–421. [CrossRef]
44. Kozlowska, M.; Goclon, J.; Rodziewicz, P. Intramolecular Hydrogen Bonds in Low-Molecular-Weight Polyethylene Glycol. *ChemPhysChem* **2016**, *17*, 1143–1153. [CrossRef]
45. Zhijiang, C.; Chengwei, H.; Guang, Y. Crystallization behavior, thermal property and biodegradation of poly(3-hydroxybutyrate)/poly(ethylene glycol) grafting copolymer. *Polym. Degrad. Stab.* **2011**, *96*, 1602–1609. [CrossRef]
46. Andrade, K.L.; Ramlow, H.; Floriano, J.F.; Acosta, E.D.; Faita, F.L.; Machado, R.A.F. Latex and natural rubber: Recent advances for biomedical applications. *Polimeros* **2022**, *32*, e2022015. [CrossRef]
47. Wang, H.; Feng, Y.; Fang, Z.; Yuan, W.; Khan, M. Co-electrospun blends of PU and PEG as potential biocompatible scaffolds for small-diameter vascular tissue engineering. *Mater. Sci. Eng. C* **2012**, *32*, 2306–2315. [CrossRef]
48. Llorens, E.; Bellmunt, S.; del Valle, L.J.; Puiggalí, J. Scaffolds constituted by mixed polylactide and poly(ethylene glycol) electrospun microfibers. *J. Polym. Res.* **2014**, *21*, 603. [CrossRef]
49. Kiani, S.; Mousavi, S.M.; Shahtahmassebi, N.; Saljoughi, E. Hydrophilicity improvement in polyphenylsulfone nanofibrous filtration membranes through addition of polyethylene glycol. *Appl. Surf. Sci.* **2015**, *359*, 252–258. [CrossRef]
50. Ma, G.; Yang, D.; Wang, K.; Han, J.; Ding, S.; Song, G.; Nie, J. Organic-soluble chitosan/polyhydroxybutyrate ultrafine fibers as skin regeneration prepared by electrospinning. *J. Appl. Polym. Sci.* **2010**, *118*, 3619–3624. [CrossRef]